Quantum simulations of ultracold molecules

Brendan Abolins, *b.abolins@berkeley.edu*

August 31, 2010

Abstract

Ultracold molecules are at the forefront of efforts to explore novel many-body phenomena, offering a great deal of control over the nature and strength of intermolecular interactions through the application of external electric and magnetic fields. As the experimental techniques mature there becomes a need to develop theoretical models to understand the phenomenon which are observed. One such technique is path integral ground state Monte Carlo (PIGSMC) which is an exact ground state method which is capable of calculating properties of interacting many-body systems without employing uncontrolled approximations. The development of a PIGSMC code capable of simulating a system composed fully of interacting rigid dipoles, the first of its kind, is presented along with some preliminary results of its application to toy systems is presented, showing excellent agreement between Monte Carlo simulation and variational and perturbation theory results.

Contents

1 Introduction **1**
1.1 Quantum Monte Carlo 2

2 PIGSMC for point dipoles **6**
2.1 Sixth order short time propagator 6
2.2 Single bead and multibead trial moves 8

3 Results **12**
3.1 Single dipole in a constant electric field 12
3.2 Two dipoles fixed in space with the dipole-dipole interaction 15
3.3 Systems of many stationary dipoles 17

4 Conclusion and outlook **19**

Acknowledgments **19**

References **19**

1 Introduction

Ultracold molecules have a tremendous amount to offer to many fields of physics. Their interactions, which are long ranged in nature, can be controlled through careful tuning of

external electric and magnetic fields, making molecules at ultracold temperatures valuable for studying novel many-body physics. This tunability can also be exploited to explore chemical reactions at ultracold temperatures by controlling precisely the quantum state of the reactants and products [6]. Ultracold molecules also have the potential applications in quantum information processing, as the controllability makes it possible to manipulate the internal state of the molecules relatively easily and the long-ranged interactions can be exploited to entangle qubits [5]. For a review of applications of ultracold molecules see [2].

Calculations to this point have largely been restricted to systems of dipoles in external, aligning fields due to the difficulty of incorporating the internal (rotational) degrees of freedom. This leaves open questions regarding the interplay of these internal degrees of freedom and the external (translational) degrees of freedom which are coupled through the anisotropic long-ranged dipole-dipole interaction in dipolar molecules. Answering these questions requires a method which can treat the full many-body Hamiltonian for a system of interacting molecules with rotational degrees of freedom; quantum Monte Carlo is such a method.

1.1 Quantum Monte Carlo

In general, for an interacting many-body system, it is extremely difficult or even impossible to formulate analytical solutions to the time-independent Schrödinger equation. Even if it were possible to write down an analytical expression for the many-body wavefunction for a system of N point particles the calculation of expectation values, $\langle O \rangle$, will involve the evaluation of $3N$ dimensional integrals of the form $\int dR\, \Psi(R)^* O(R) \Psi(R)$ for some operator $\hat{O}$. This is itself incredibly challenging if $\Psi(R)$ is not of a convenient, easy to evaluate form.

Quantum Monte Carlo (QMC) methods aim to solve one or both of these challenges. At their core most Monte Carlo methods simply use Monte Carlo integration to evaluate the many dimensional integrals that arise in many-body physics. The simplest of these QMC methods is variational Monte Carlo which is simply the variational method applied to the many-body problem where the expectation value of the energy is computed using Monte Carlo integration. The many-body Hamiltonian for a generic system of N interacting particles in an external potential is given by

$$\hat{H} = \sum_{i=1}^{N} \lambda \nabla_i^2 + \sum_{i=1}^{N} V_{ext}(\hat{r}_i) + \sum_{i<j} V_{int}(\hat{r}_i, \hat{r}_j) \tag{1}$$

where $\lambda = -\hbar^2/2m$ and $\hat{r}_i$ is the position operator for particle i. In variational Monte Carlo (VMC) the goal is to minimize the expectation value of the energy given by

$$\langle E \rangle = \frac{\int d\mathbf{R}\ |\Psi_T(\mathbf{R})|^2 E_L(\mathbf{R})}{\int d\mathbf{R}\ |\Psi_T(\mathbf{R})|^2} \tag{2}$$

$$E_L(\mathbf{R}) = \frac{1}{\Psi_T(\mathbf{R})} \hat{H} \Psi_T(\mathbf{R}) \tag{3}$$

given a trial wavefunction $\Psi_T(\mathbf{R})$ which contains variational parameters, where $\mathbf{R}$ represents all $3N$ coordinates of the N-body system and $E_L(\mathbf{R})$ is known as the local energy

of the system. Typically the trial wavefunction is of the form

$$\Psi_T(\mathbf{R}) = \prod_{i=1}^{N} \phi(r_i) \prod_{i<j} f(r_i, r_j) \tag{4}$$

which accounts for one- and two-body effects, though it is possible to add functions involving three or more particles to capture the effects of more complicated correlations. By minimizing the expectation value in equation (2) through the variation of parameters in the one- and two- (or more) body functions one arrives at an upper bound to the ground state energy.

The integral in equation (2) is evaluated by Monte Carlo integration (hence the Monte Carlo) in which the integral is approximated by

$$\langle E \rangle = \frac{1}{M} \sum_{i=1}^{M} E_L(\mathbf{R}_i) \tag{5}$$

where the M configurations $\mathbf{R}_i$ are chosen randomly from the distribution $|\Psi_T(\mathbf{R})|^2$. To do this the Metropolis algorithm described in ref. [7], a form of importance sampling, is employed. With the Metropolis algorithm new configurations are generated from the old through a Markov process. The probability of transitioning from a configuration $\mathbf{R}_i$ to a new configuration $\mathbf{R}_j$ is given by

$$M_{ji} = A_{ji} T_{ji} \tag{6}$$

where M is the transition matrix, A represents the probability of transitioning from configuration $\mathbf{R}_i$ to configuration $\mathbf{R}_j$ and T is the transfer matrix which is the rule for generating a new configuration from the old. The probability of a given state P_i is given by

$$P_i = \sum_j M_{ij} P_j \tag{7}$$

and that the sum $\sum_j M_{ij} = 1$. If the condition of detailed balance is assumed, that is $A_{ij} T_{ij} P_j = A_{ji} T_{ji} P_i$, then a common choice for the acceptance matrix connecting a state $\mathbf{R}_i$ to a state $\mathbf{R}_j$ is given by

$$A_{ji} = \min\left(\frac{P_j T_{ij}}{P_i T_{ij}}, 1\right) \tag{8}$$

which is usually simplified by choosing the transfer matrix such that $T_{ij} = T_{ji}$. Then the probability of accepting a move from one configuration to the next only depends on the relative probabilities of each of the configurations.

Applying this algorithm to VMC is straightforward and proceeds as follows:

1. A particle i is chosen at random
2. Its position is updated as $\vec{r_i}' = \vec{r_i} + \sigma\vec{\xi}$ where $\vec{\xi}$ is chosen for instance from a symmetric distribution such as the uniform distribution over the interval -1 to 1, $U[-1, 1]$, or the standard normal distribution, $N[0, 1]$.
3. the acceptance matrix element is calculated, $A \leftarrow \min(|\Psi_T(\mathbf{R}')|^2 / |\Psi_T(\mathbf{R})|^2, 1)$
4. a random number ξ is chosen from $U[0, 1]$ and the new configuration $\mathbf{R}'$ is accepted if $A > \xi$ and rejected otherwise.

5. The average energy is updated and the process is repeated.

The quantities computed from VMC are, however, only approximations to true ground state properties. In order to exactly calculate ground state properties it is necessary to go beyond the variational method and in the present work this is done with path integral ground state Monte Carlo. Path integral ground state Monte Carlo (PIGSMC, also known as variational path integral Monte Carlo or VPIMC) is an exact ground state method in which a guiding wavefunction, for instance, the optimized output from a VMC calculation, is propagated in imaginary time. The quantum mechanical propagator for a given (time independent) Hamiltonian $\hat{H}$ is

$$\hat{G}(t) = e^{-i\hat{H}t/\hbar} \tag{9}$$

which describes the evolution of a quantum system from an initial time 0 to a final time t. Imaginary time propagation is accomplished through the substitution $t \to -i\tau$.

In general the guiding wavefunctions employed can be expressed, formally, as a linear combination of the exact eigenstates of the Hamiltonian under investigation

$$|\Psi_T\rangle = \sum_i c_i |\Phi_i\rangle \tag{10}$$

where the expansion coefficients are $c_i = \langle\Phi_i|\Psi_T\rangle$. The propagator, either in real or imaginary time, can similarly be expanded in terms of the exact eigenstates of the Hamiltonian

$$\hat{G}(\beta/2) = \sum_i e^{-\beta E_i/2\hbar} |\Phi_i\rangle\langle\Phi_i| \tag{11}$$

where E_i is the energy of state $|\Phi_i\rangle$. When the imaginary time propagator is applied to the guiding wavefunction

$$\hat{G}(\beta/2)|\Psi_T\rangle = \sum_i c_i e^{-\beta E_i/2\hbar} |\Phi_i\rangle \tag{12}$$

the results is evolution of the guiding wavefunction toward the ground state of the Hamiltonian in the limit that $\beta/2 \to \infty$ provided $|\Psi_T\rangle$ has non-zero overlap with the ground state ($c_0 \neq 0$). This can easily be seen as the contribution of state i to the guiding wavefunction after a propagation period of ϵ in imaginary time is $c_i e^{-\epsilon E_i/\hbar}$, a decaying exponential with a mean lifetime of $\hbar/E_i$ which is longest for the ground state. The ground state (aside from normalization) is thus given by

$$|\Phi_0\rangle = \hat{G}(\beta/2)|\Psi_T\rangle \tag{13}$$

in the long imaginary time limit. Ground state expectation values can be expressed in a similar manner. For a generic operator $\hat{O}$ the expectation value is given by

$$\langle O\rangle = \frac{\langle\Phi_0|\hat{O}|\Phi_0\rangle}{\langle\Phi_0|\Phi_0\rangle} \tag{14}$$

$$= \frac{\langle\Psi_T|\hat{G}(\beta/2)\hat{O}\hat{G}(\beta/2)|\Psi_T\rangle}{\langle\Psi_T|\hat{G}(\beta/2)\hat{G}(\beta/2)|\Psi_T\rangle} \tag{15}$$

for a sufficiently long propagation time.

However, in general the neither the expansion of the guiding state in terms of the

eigenstates of the Hamiltonian nor the expansion of the propagator in terms of the same is known *a priori*. In order to get around this it is necessary to make some controlled approximations. It is convenient to proceed in the coordinate representation where

$$G(\mathbf{R}, \mathbf{R}', \beta/2) = \langle \mathbf{R}|\hat{G}(\beta/2)|\mathbf{R}'\rangle \tag{16}$$

and

$$\Psi_T(\mathbf{R}) = \langle \mathbf{R}|\Psi_T\rangle \tag{17}$$

are the expressions for the propagator and guiding wavefunction (and an expression for any other wavefunction can be formulated analogously). Evaluating the exact propagator in the coordinate representation is non-trivial and is tantamount to solving exactly the many-body problem. It is possible, however, to write down expressions for the kinetic energy and potential energy portions of the propagator, $e^{-\tau\hat{T}/\hbar}$ and $e^{-\tau\hat{V}/\hbar}$ respectively, separately since the former is diagonal in k-space and the latter is diagonal in real space. Through Taylor expansion of the propagator about the point $\tau = 0$ one can show for sufficiently small τ that

$$e^{-\tau(\hat{T}+\hat{V})/\hbar} = e^{-\tau\hat{T}/\hbar}e^{-\tau\hat{V}/\hbar} + O(\tau^2) \tag{18}$$

or that

$$e^{-\tau(\hat{T}+\hat{V})/\hbar} = e^{-\tau\hat{V}/2\hbar}e^{-\tau\hat{T}/\hbar}e^{-\tau\hat{V}/2\hbar} + O(\tau^3) = \hat{G}_2(\tau) \tag{19}$$

which is known as the primitive approximation to the propagator. By themselves neither of these approximations is particularly useful since equation (13) is only exact for a good approximation in the long imaginary time limit where these short imaginary time approximations are not valid but it is exactly true that

$$e^{-\beta\hat{H}/2\hbar} = \left(e^{-\tau\hat{H}/\hbar}\right)^M \tag{20}$$

where $\tau M = \beta/2$. In this way a long path of length $\beta/2$ can be decomposed into a sequence of short path segments of length τ where τ is short enough for equation (19) to hold.

The expression for the expectation value of an operator is then

$$\langle O\rangle = \frac{\langle\Psi_T|(\hat{G}_2(\tau))^M\hat{O}(\hat{G}_2(\tau))^M|\Psi_T\rangle}{\langle\Psi_T|(\hat{G}_2(\tau))^{2M}|\Psi_T\rangle} + O(\tau^2) \tag{21}$$

where the error is one order less since M is on the order of $1/\tau$. The expression used in PIGSMC is arrived at by inserting the identity in between each short time propagator, breaking the path into a series of discrete *time slices* which are composed of *beads*, where a bead is the position of a particle at a given time slice. This is given (ignoring the normalization which is inconsequential in Monte Carlo methods) by

$$\begin{aligned}\langle O\rangle = \int d\mathbf{R}_0 \ldots d\mathbf{R}_{2M}\Psi_T(\mathbf{R}_0)G_2(\mathbf{R}_0, \mathbf{R}_1, \tau)\ldots G_2(\mathbf{R}_{M-1}, \mathbf{R}_M, \tau)O(\mathbf{R}_M) \\ \times G_2(\mathbf{R}_M, \mathbf{R}_{M+1}, \tau)\ldots G_2(\mathbf{R}_{2M-1}, \mathbf{R}_{2M}, \tau)\Psi_T(\mathbf{R}_{2M})\end{aligned} \tag{22}$$

which can be evaluated by Monte Carlo integration in a fashion analogous to VMC. In PIGSMC, however, instead of the probability of a configuration being given by $|\Psi_T(\mathbf{R})|^2$,

the probability of a *path* is given by

$$P(\mathbf{R}_0, \ldots, \mathbf{R}_{2M}) = \Psi_T(\mathbf{R}_0) G_2(\mathbf{R}_0, \mathbf{R}_1, \tau) \ldots G_2(\mathbf{R}_{2M-1}, \mathbf{R}_{2M}, \tau) \Psi_T(\mathbf{R}_{2M}) \tag{23}$$

and sums like the one in equation (5) are then over randomly selected paths. For most quantities the expectation value is calculated using the configurations at the center time slice, which, provided $\beta/2$ is long enough, are distributed according to the ground state wavefunction. The exception to this is the energy (or any other operator which commutes with the Hamiltonian) which is evaluated at the ends of the paths. For example, in PIGSMC the energy expectation is still calculated through the local energy at either end of the path.

This outlines the PIGSMC method for a system of interacting point particles. The next step is to extend this to method to handle particles with rotational degrees of freedom.

2 PIGSMC for point dipoles

In order to study systems with rotational degrees of freedom using PIGSMC, a short time propagator for the rotational degrees of freedom must be developed. In addition, single- and multibead trial moves of the rotational degrees of freedom must be developed in analogy to the methods used for translational degrees of freedom.

2.1 Sixth order short time propagator

In order to study the many-body physics of systems of molecules using the path integral ground state Monte Carlo method a code which incorporates rotations must be developed. The Hamiltonian describing a system of N dipoles with rotational degrees of freedom in addition to the usual translational degrees if freedom is

$$\hat{H} = \sum_{i=1}^{N} \left(\lambda \nabla_i^2 + B \hat{L}_i^2 \right) + \sum_{i=1}^{N} V_{ext}(\hat{r}_i) + \sum_{i<j} V_{int}(\hat{r}_i, \hat{r}_j) \tag{24}$$

where $B = \hbar^2/2I$, and the $\hat{r}_i$'s are now the operators corresponding to all of the coordinates, describing both position and orientation, of molecule i. The potential energy terms have the effect of coupling the translational and rotational motions of the molecules in non-trivial ways.

As described previously, an approximation to the short time propagator in imaginary time must be formulated. Fortunately the rotational and translational kinetic energy operators commute and so the exact imaginary time propagator for the rigid rotor free particle is

$$\hat{G}_{free} = e^{-\tau(\lambda\nabla^2 + B\hat{L}^2)/\hbar} = e^{-\tau\lambda\nabla^2/\hbar} e^{-\tau B\hat{L}^2/\hbar} = \hat{\rho}_{trans}\hat{\rho}_{rot} \tag{25}$$

which clearly shows that in the absence of a potential term the rotations and translations of the molecules in the system are independent. This property makes it obvious that the extension of the primitive approximation to the short time propagator which includes rotational degrees of freedom is simply

$$\hat{G} = \hat{G}_2 + O(\tau^3) = e^{-\tau\hat{V}/2} \hat{\rho}_{trans} \hat{\rho}_{rot} e^{-\tau\hat{V}/2} + O(\tau^3) \tag{26}$$

where $\hat{V}$ is the quantum mechanical total potential energy operator and $\hbar = 1$. This expression will be the basis for all further approximations to the short time propagator.

In order to explore longer imaginary propagation times, β in a reasonable amount of computer time it is beneficial to implement higher order approximations to the short time propagator. In the present work a sixth order approximation to the short time propagator was implemented through a multi-product expansion of the short time propagator [4]. Given a set of n whole numbers k_i, the propagator of order $2n$ can be expressed as

$$\hat{G} = \hat{G}_{2n}(\tau) + O(\tau^{2n+1}) = \sum_{i=1}^{n} c_i (\hat{G}_2(\tau/k_i))^{k_i} + O(\tau^{2n+1}) \tag{27}$$

$$c_i = \prod_{j \neq i} \frac{k_i^2}{k_i^2 - k_j^2} \tag{28}$$

where $\hat{G}_2(\epsilon)$ is the second order propagator, equation (26), with small time step ϵ. As per the suggestion in ref. [10] the set $\{k_i\} = \{1, 2, 4\}$ was used for the implementation of the sixth order propagator. This gives for the sixth order propagator

$$\hat{G}_6(4\tau) = \frac{1}{45}\hat{G}_2(4\tau) - \frac{4}{9}(\hat{G}_2(2\tau))^2 + \frac{64}{45}(\hat{G}_2(\tau))^4 \tag{29}$$

$$\begin{aligned} &= \frac{1}{45} e^{-2\tau\hat{V}} \hat{\rho}(4\tau) e^{-2\tau\hat{V}} - \frac{4}{9} e^{-\tau\hat{V}} \hat{\rho}(2\tau) e^{-2\tau\hat{V}} \hat{\rho}(2\tau) e^{-\tau\hat{V}} \\ &\quad + \frac{64}{45} e^{-\tau\hat{V}/2} \hat{\rho}(\tau) e^{-\tau\hat{V}} \hat{\rho}(\tau) e^{-\tau\hat{V}} \hat{\rho}(\tau) e^{-\tau\hat{V}} \hat{\rho}(\tau) e^{-\tau\hat{V}/2} \end{aligned} \tag{30}$$

where $\hat{\rho} = \hat{\rho}_{trans}\hat{\rho}_{rot}$ are the free particle propagators for particles with rotational degrees of freedom. This can be further simplified by recognizing that $\hat{\rho}(4\tau) = (\hat{\rho}(\tau))^4$ and inserting the resolution of the identity. In the coordinate representation this is then

$$\begin{aligned} \langle \mathbf{R}_1 | \hat{G}_6(4\tau) | \mathbf{R}_5 \rangle = &\int d\mathbf{R}_2 \int d\mathbf{R}_3 \int d\mathbf{R}_4 \, \langle \mathbf{R}_1 | \hat{\rho}(\tau) | \mathbf{R}_2 \rangle \langle \mathbf{R}_2 | \hat{\rho}(\tau) | \mathbf{R}_3 \rangle \\ &\times \langle \mathbf{R}_3 | \hat{\rho}(\tau) | \mathbf{R}_4 \rangle \langle \mathbf{R}_4 | \hat{\rho}(\tau) | \mathbf{R}_5 \rangle F(\mathbf{R}_1, \mathbf{R}_2, \mathbf{R}_3, \mathbf{R}_4, \mathbf{R}_5, \tau) \end{aligned} \tag{31}$$

$$\begin{aligned} F(\mathbf{R}_1, \mathbf{R}_2, \mathbf{R}_3, \mathbf{R}_4, \mathbf{R}_5, \tau) = &\frac{1}{45} e^{-2\tau(V(\mathbf{R}_1)+V(\mathbf{R}_5))} - \frac{4}{9} e^{-\tau(V(\mathbf{R}_1)+2V(\mathbf{R}_3)+V(\mathbf{R}_5))} \\ &+ \frac{64}{45} e^{-\tau(V(\mathbf{R}_1)+2V(\mathbf{R}_2)+2V(\mathbf{R}_3)+2V(\mathbf{R}_4)+V(\mathbf{R}_5))/2} \end{aligned} \tag{32}$$

with $\mathbf{R}_i$ representing all of the coordinates (both translational and rotational) of the many-body system at time slice i. In this form the propagator is ready for use in a PIGSMC code. It should be noted, however, that each time slice in imaginary time is now made up of four time slices which are one fourth as long. When one of the "sub" time slices is updated an evaluation of the potential on each of the other 4 time slices is required in order to evaluate the propagator. At first this seems incredibly inefficient but this can largely be remedied by storing the potential energy at each time slice in an array and simply recalling these values as necessary, and only recalculating the potential energy for slices which are actually updated. This, too, can be made less computationally costly by only calculating interactions which have changed. If only single particles are updated at a time this is simply an $O(N)$ operation instead of the $O(N^2)$ operation required to calculate the entire potential again.

Now all that remains is to calculate each of the terms in the expression above. F is

the simplest to calculate since the potential energy, as well as it's exponential, is diagonal in the coordinate representation. With $\hat{\rho}$ it is easiest to consider the translational and rotational parts separately. The translational portion, $\hat{\rho}_{trans}$, is not diagonal in the coordinate representation, but it is diagonal in the momentum representation. Through insertion of a complete set of states in momentum space it is possible to arrive at the exact form of the free particle propagator

$$\langle \mathbf{R}_1 | \hat{\rho}_{trans}(\tau) | \mathbf{R}_2 \rangle = (4\pi\lambda\tau)^{-3N/2} e^{-(\mathbf{R}_2 - \mathbf{R}_1)^2/4\lambda\tau} \tag{33}$$

but it should be noted that in this expression $\mathbf{R}_i$ is now only the translational coordinates of the N particle system. This just leaves the propagator for the free rotor. This propagator, again, is not diagonal in the coordinate representation but is in fact diagonal in the angular momentum representation. Derivation of a coordinate representation expression for the free rotor propagator proceeds in the same way as for the free particle propagator, through an insertion of a complete set of angular momentum states. This results in

$$\langle \mathbf{\Omega}_1 | \hat{\rho}_{rot}(\tau) | \mathbf{\Omega}_2 \rangle = \prod_{i=1}^{N} \sum_{l=0}^{\infty} \frac{2l+1}{4\pi} P_l(\omega_1^i \cdot \omega_2^i) e^{-\tau B l(l+1)} \tag{34}$$

with $\mathbf{\Omega}_i$ representing the orientations of all of the N particles at time slice i and ω_i^j representing the orientation of particle j at time slice i. This expression can not be simplified any further but since the sum converges it can be calculated to any desired accuracy by truncating the sum at a sufficiently high l as suggested in ref. [8]. This is then calculated once on a discrete grid in the angle between two orientations from 0 to π at the beginning of the simulation and then values are looked up when needed.

And those are all of the elements needed to implement a higher order approximation to the short time propagator. In the current work a sixth order propagator was implemented for rotations but it doesn't need to stop there. In principle an approximation to any order can be formulated using these elements. for instance if one instead chooses $\{k_i\} = \{1, 2, 3, 6\}$ then one arrives at an eighth order propagator. This could be done to any desired accuracy; for a more complete discussion of these multi-product expansion propagators see ref. [10].

2.2 Single bead and multibead trial moves

In order to calculate estimates of various properties of a system as well as estimates of the error in those estimates it is necessary to generate a great many independent paths of the system under investigation through imaginary time. This means having an efficient way of generating new configurations which vary significantly from the old configurations.

A simple, albeit inefficient, method for generating new configurations is the single bead move where the coordinates of a single particle at a single time slice are perturbed randomly to generate a new configuration. Since each new path only differs from the previous by a single coordinate many paths must be generated before memory of a previous path has significantly decayed. It is, however, relatively easy to implement and a good starting point as well as fallback move for more complicated move types. It was for this reason that it was the first type of move implemented for rotations of particles in the present work.

The heart of the single bead move algorithm is the generation of the trial move. In

principle one can choose any type of trial move desired. For translations commonly a random displacement is chosen from the uniform distribution centered around the current configuration, or from a Gaussian centered around the current configuration. The choice of distribution from which to draw random displacements affects the acceptance ratio and as such can affect the efficiency of the sampling algorithm. If the acceptance ratio is too high then the sampled points likely don't vary from one another enough and configurations are likely to be highly correlated. If the acceptance ratio is too low then the configurations do not change very often and again they tend to be highly correlated. A good rule of thumb is to aim for an acceptance ratio between 30% and 70% by, for example, tuning the width of the Gaussian or uniform distribution.

Generating new translational configuration is relatively straightforward. For example, new configurations could be generated simply by adding a random vector whose elements are distributed according to a desired distribution. This is not the case with sampling orientations, the key difference being that orientations of linear molecular rotors necessarily reside on the surface of a sphere. It is then necessary to generate not random displacements, but random rotations of the orientations, for example, through the use of randomly generated rotation matrices. These rotation matrices, however, are hard to visualize and implement and so in the current work a different method for generating random rotations was sought.

Ultimately, random unit quaternions were the representation of choice for random rotations. A unit quaternion which represents a rotation has the structure

$$\mathbf{q} = \cos(\alpha/2) + \sin(\alpha/2)\vec{v} \tag{35}$$

where $\vec{v}$ is a unit vector and is the axis about which the rotation is performed and α is the angle of the rotation. For point dipoles where the orientation is completely determined by two coordinates, θ and ϕ, the angle α is the angle of the rotation only when $\vec{v}$ is perpendicular to the orientation of the point dipole. This is because rotation about the axis collinear with the dipole orientation doesn't change the orientation of the dipole. As such, for the current work, the vector $\vec{v}$ is restricted to the plane perpendicular to the dipole orientation when formulating trial moves.

The generation of a random number rotation by the generation of a random unit quaternion requires four random numbers. These numbers are chosen from from a normal distribution with zero mean and unit variance. This ensures that the rotational axes are uniformly distributed on the unit sphere and provides an acceptable acceptance ratio when the Gaussian from which the rotation angle, α, is drawn is scaled to have variance $2B\tau$ and restricted to the interval $0 \leq \alpha \leq \pi$; it should be noted that because of the differential area element on a sphere this means that the probability $P(\alpha) \propto e^{-\alpha^2/4B\tau}/\sin(\alpha)$ for $0 \leq \alpha \leq \pi$ and 0 otherwise. To ensure that the rotation axis is always perpendicular to the dipole orientation, the orthogonal projection of the rotation axis on the dipole orientation is subtracted from the rotation axis vector before normalization.

Once the random unit quaternion is constructed it is necessary to convert the quaternion into a rotation matrix. The relationship between unit quaternions and orthogonal

matrices which represent rotations is

$$\mathbf{q} = a + b\,\hat{\imath} + c\,\hat{\jmath} + d\,\hat{k} \tag{36}$$

$$\mathbf{R} = \begin{pmatrix} a^2+b^2-c^2-d^2 & 2bc-2ad & 2bd+2ac \\ 2bc+2ad & a^2-b^2+c^2-d^2 & 2cd-2ab \\ 2bd-2ac & 2cd+2ab & a^2-b^2-c^2+d^2 \end{pmatrix} \tag{37}$$

which can then be multiplied with the unit vector which represents the dipole orientation to effect a rotation of that dipole orientation.

The single bead move for rotations then proceeds as follows:

1. Pick a bead, ω_i^j, at random.
2. Generate random unit quaternion, $\mathbf{q}$ and convert it into a rotation matrix $\mathbf{R}$.
3. Generate a new orientation according to $\vec{\omega}_i'^j \leftarrow \mathbf{R} \cdot \vec{\omega}_i^j$.
4. Calculate the acceptance probability as $A \leftarrow \min(1, \pi'/\pi)$.
5. Accept or reject the new orientation with probability A.

These single bead moves serve as an illustrative introduction to the sampling of orientations but the algorithm samples paths very slowly. Moves which update multiple beads at once are desirable as they not only result in paths which are more different from one iteration to the next, but they also allow for larger amplitude trial displacements which again increases the rate of diffusion through the space of possible paths. A good discussion of the reasons for this as well as a description of the multilevel bisection algorithm implemented in the current work can be found in ref. [3].

The key advantages of the multilevel bisection algorithm over other multibead type moves is the possibility of early rejection. With this, large amplitude moves which result in unfavorable configurations are recognized and rejected early. This prevents full calculations of the propagator for paths which are likely to be rejected anyway, saving computational time and enabling a quicker sampling of the most important paths.

The multilevel bisection algorithm proceeds as follows. First a particle and section of path are chose. This section of path should contain a number of intervals which is a power of two; for the sake of further discussion this will be taken to be 8 time intervals long but could, in general, be any length. From the beads, labeled 1 through 9, first we propose a large trial move of the midpoint, bead 5. We calculate the acceptance probability as we would for a single bead move but use a propagator for an interval that has a length of 4τ. If this move is accepted we then propose moves in a similar fashion for the two midpoints of the two sub intervals on either side of bead 5, beads 3 and 7. We proceed until we've moved all of the beads 2 through 8 when we calculate a final acceptance ratio and either accept or reject the entire trial move. If we reject at one of the earlier stages then we start the process all over again.

Just like in the single bead case there are a variety of different types of trial moves for the individual beads and the objective is to attain a reasonable acceptance rate for each level of the algorithm. For translational moves it is customary to use a Gaussian distributed where the mean coincides between the midpoint of the two ends of the sub path $\bar{\mathbf{R}}_n = (\mathbf{R}_{n-2^{l_{max}-l}} + \mathbf{R}_{n+2^{l_{max}-l}})/2$ and a variance of $2^{l_{max}-l+1}\lambda\tau$ where l is the "level" of the move and l_{max} is the maximum level (*e.g.* l is 1 and l_{max} is 3 for the trial move of bead 5 in the example above). It can be seen, then, that the moves proposed at the center

of the sub path are potentially much larger than the moves proposed in the single bead case resulting in a quicker sampling of the possible paths. In order to fulfill the condition of detailed balance one must take care in calculating the acceptance probability. The acceptance probability, for example, at level 2 for the move $\{\bar{\mathbf{R}}'_3, \bar{\mathbf{R}}'_7\} \to \{\mathbf{R}''_3, \mathbf{R}''_7\}$ is

$$A = \min\left(1, \frac{\Delta_2}{\Delta_1} \prod_{i=3,7} \frac{T(\bar{\mathbf{R}}_i \to \mathbf{R}_i)}{T(\bar{\mathbf{R}}'_i \to \mathbf{R}''_i)}\right) \tag{38}$$

$$\Delta_1 = \frac{G(\mathbf{R}_1, \mathbf{R}'_5, 4\tau) G(\mathbf{R}_1, \mathbf{R}'_5, 4\tau)}{G(\mathbf{R}_1, \mathbf{R}_5, 4\tau) G(\mathbf{R}_5, \mathbf{R}_9, 4\tau)} \tag{39}$$

$$\Delta_2 = \frac{G(\mathbf{R}_1, \mathbf{R}''_3, 2\tau) G(\mathbf{R}''_3, \mathbf{R}'_5, 2\tau) G(\mathbf{R}'_5, \mathbf{R}''_7, 2\tau) G(\mathbf{R}''_7, \mathbf{R}_9, 2\tau)}{G(\mathbf{R}_1, \mathbf{R}_3, 2\tau) G(\mathbf{R}_3, \mathbf{R}_5, 2\tau) G(\mathbf{R}_5, \mathbf{R}_7, 2\tau) G(\mathbf{R}_7, \mathbf{R}_9, 2\tau)} \tag{40}$$

assuming, of course, that neither slice 1 nor slice 9 are at the ends of the path in which case Δ_l must be modified by multiplying by the appropriate factors of Ψ_T; Δ_0 is taken to be 1. In this case T is the process which generates the new configuration from the old which is the Gaussian with mean $\bar{\mathbf{R}}$ and variance $2^{l_{max}-l+1}\lambda\tau$ in this case, and $G(\mathbf{R}, \mathbf{R}', \tau) = \langle \mathbf{R}|\hat{G}(\tau)|\mathbf{R}'\rangle$ is the appropriate short time propagator. Also, to save computational time, a lower order, and less complicated, approximation to the short time propagator (*e.g.* using $\hat{G}_2$ instead of $\hat{G}_6$) can be used for all levels aside from l_{max}.

Just as with the single bead move this algorithm can be implemented for rotations simply by taking the translational algorithm and making a couple of minor modifications. The new orientations are constructed through the use of random unit quaternions. However, with rotations the concept of a configuration which is the midpoint of the two endpoints must be considered more carefully. Since all of the orientations lie on the surface of a unit sphere the midpoint is now the the midpoint of the circular arc connecting the endpoints ω_a^j and ω_c^j. If these orientations are not anti-parallel to one another then this midpoint is well defined and is $\bar{\omega}_b^j = (\vec{\omega}_a^j + \vec{\omega}_c^j)/\|\vec{\omega}_a^j + \vec{\omega}_c^j\|$. If the angle between endpoint orientations is π then this midpoint is not unique and it is possible to choose any vector perpendicular to the two endpoint orientations as the midpoint. The width of the distribution from which the rotational angle is drawn is varied in a way analogous to the width of the Gaussian distribution in the case of translational moves but it should be stressed that, as stated before, T is not a Gaussian but is $\propto e^{-\alpha^2/2^{l_{max}-l+1}B\tau}/\sin(\alpha)$ for $0 \leq \alpha \leq \pi$ and 0 otherwise, where $\alpha = \arccos(\bar{\omega}_b^j \cdot \vec{\omega}_b^j)$.

The multilevel bisection algorithm for rotations is then:

1. Pick a particle label j and range of beads of length $2^{l_{max}+1}$ at random.
2. Begin at level 1. For each sub interval
   (a) Calculate the midpoint $\bar{\omega}_b^j$.
   (b) Generate a random unit quaternion $\mathbf{q}$ and convert it to the equivalent rotation matrix $\mathbf{R}$.
   (c) Generate the new orientation according to $\vec{\omega}_b'^j \leftarrow \mathbf{R} \cdot \bar{\omega}_b^j$.
3. Calculate the acceptance probability at the current level, A, in the appropriate manner.
4. Accept or reject the new path with probability A.

5. If the move is accepted and the current level is not l_{max} then return to step 2 for the next level.

Additional move types may be desirable, such as a move in which all beads with a given particle label are rigidly displaced (or rotated) in some uniform fashion but this is essentially a special case of the single bead move and is just as easy to formulate.

With these elements, a short time propagator with rotational and translational contributions and a variety of trial bead moves, systems of particles which interact through some orientation dependent potential energy are accessible to study.

3 Results

In the long run the code developed in the current work will be applied to problems in which rotational and translational degrees of freedom are coupled together. As a step in that direction the code will initially be applied to systems which have rotational degrees of freedom but are strongly polarized in one direction. For instance there has been some theoretical investigation of systems of oriented dipoles in 3 dimensions in which the $1/r^3$ nature of the dipole-dipole interaction is truly long-ranged. Such systems exhibit novel structure [9] but systems in which the assumption of perfect alignment is relaxed may also exhibit interesting behavior. The PIGSMC code developed over the course of this work will be able to do realistic calculations of such systems where the orientation is not frozen. However, as a test of the code, systems of interest in which only rotations played a role were sought.

3.1 Single dipole in a constant electric field

With any newly developed code it is a good idea to test it out on a problem for which it is possible to compute an exact answer. In the current case the obvious choice, a single rigid rotor, fixed in space, was considered too trivial. The most naïve guiding wavefunction, a constant wavefunction $\psi_T = const.$ is, in fact, the exact ground state wavefunction of the rigid rotor, whose states are the spherical harmonics $Y_l^m(\theta, \phi)$. The problem which was finally settled upon as a first test of the system was then the case of a single rigid rotor, fixed in space, with a dipole moment under the influence of a constant electric field.

The Hamiltonian which describes this system when the direction of the electric field is along the positive z-axis (for convenience) is

$$\hat{H} = B\hat{L}^2 - \vec{E} \cdot d\,\hat{\Omega} \tag{41}$$

$$= B\hat{L}^2 - d\,\|E\|\cos(\theta) \tag{42}$$

where B is the rotational constant of the rotor, $\|E\|$ is the magnitude of the electric field, d is the dipole moment of the rotor, and θ is the angle between the dipole orientation and the direction of the electric field. This system has a single parameter, the ratio of the rotational constant, B, and the interaction strength, $d\,\|E\|$. This highlights the competition of the kinetic energy which, through the uncertainty principle, has the effect of delocalizing the orientation, and the potential energy which has the opposite effect. Clearly in the limit when $B/d\,\|E\| \to \infty$ the kinetic energy wins and we recover the free rigid rotor again. The opposite limit, when $B/d\,\|E\| \to 0$ corresponds to the classical

limit in which the dipole tends to be perfectly aligned along the electric field. Non-trivial behavior occurs in between these two extremes.

In 3 dimensions analytical solutions to the time independent Schrödinger equation $\hat{H}|\psi\rangle = E|\psi\rangle$ are not forthcoming. In principle, however, this is not a problem as in this space the rigid rotor states form a convenient basis for expanding the exact state in. The exact state $|\psi\rangle$ in terms of the rigid rotor states is

$$|\psi\rangle = \sum_{l=0}^{\infty} \sum_{m=-l}^{l} c_{l,m}|l,m\rangle \tag{43}$$

$$c_{l,m} = \langle l,m|\psi\rangle \tag{44}$$

$$Y_l^m(\theta,\phi) = \langle \mathbf{\Omega}|l,m\rangle \tag{45}$$

which offers some insight into how to approach the problem. Keeping in mind that the potential energy term tends to align the rotor with the field and the kinetic energy term fights against this it is clear that as the potential term gets stronger the influence of states $|l,m\rangle$ with higher kinetic energy (in other words higher l) become more important. In other words, so long as the potential energy is low compared to B then only the first few $c_{l,m}$'s should differ significantly from 0. This means it's reasonable to truncate the basis of states $|l,m\rangle$ at some l_{max}.

The problem then becomes finding the eigenvalues and eigenvectors of the matrix $\mathbf{H}$ whose elements are

$$\langle l',m'|\hat{H}|l,m\rangle = \int_0^{\pi}\int_0^{2\pi} d\theta\, d\phi\, Y_{l'}^{m'}(\theta,\phi)^*(B\hat{L}^2 + d\,\|E\|\cos(\theta))Y_l^m(\theta,\phi)\sin(\theta) \tag{46}$$

$$= Bl(l+1)\delta_{l',l}\delta_{m',m} + d\,\|E\|\sqrt{(2l'+1)(2l+1)}(-1)^{m'}\begin{pmatrix} l' & 1 & l \\ 0 & 0 & 0\end{pmatrix}\begin{pmatrix} l' & 1 & l \\ -m' & 0 & m\end{pmatrix} \tag{47}$$

where the two by by three arrays are the Wigner $3j$ symbols. It can be seen that the potential term only mixes states which differ in l but is diagonal in m because the potential energy is independent of the angle ϕ. This means that in order to calculate the energy it is only necessary to diagonalize the Hamilton in the basis $|l,0\rangle$ which simplifies equation (47) to

$$\langle l'|\hat{H}|l\rangle = Bl(l+1)\delta_{l',l} + d\,\|E\|\sqrt{(2l'+1)(2l+1)}\begin{pmatrix} l' & 1 & l \\ 0 & 0 & 0\end{pmatrix}^2 \tag{48}$$

yielding a tridiagonal matrix $\mathbf{H}$.

This result primarily served as a basis for comparison. The first step in any simulation is finding values of β and τ which are sufficiently large and small, respectively, such that properties are sampled from a state which is "close enough" to the true ground state. This entails running simulations at various values of β and τ and finding a region where the calculated ground state energy is close to the extrapolated ground state energy at $\beta \to \infty$ and $\tau \to 0$. In this case it is possible to guess what the value of β should be. Recalling that the propagation of the guiding wavefunction in imaginary time has the effect of causing the expansion coefficients of excited state contributions to decay as $e^{-\beta(E_{excited}-E_{ground})}$ (where E_{ground} is taken as the zero of energy) then it's clear that β should be related to the energy gap between the ground and first excited states if the guiding wavefunction has significant excited state character. Specifically, all things being equal, a smaller energy gap would require a longer β. In this case, finding the eigenvalues

of **H** yields not only the ground state energy but the complete spectrum of the $l_{max}+1$ lowest energy states within the truncated basis, and this first excited state energy can be used to guide an estimate for an initial value of β.

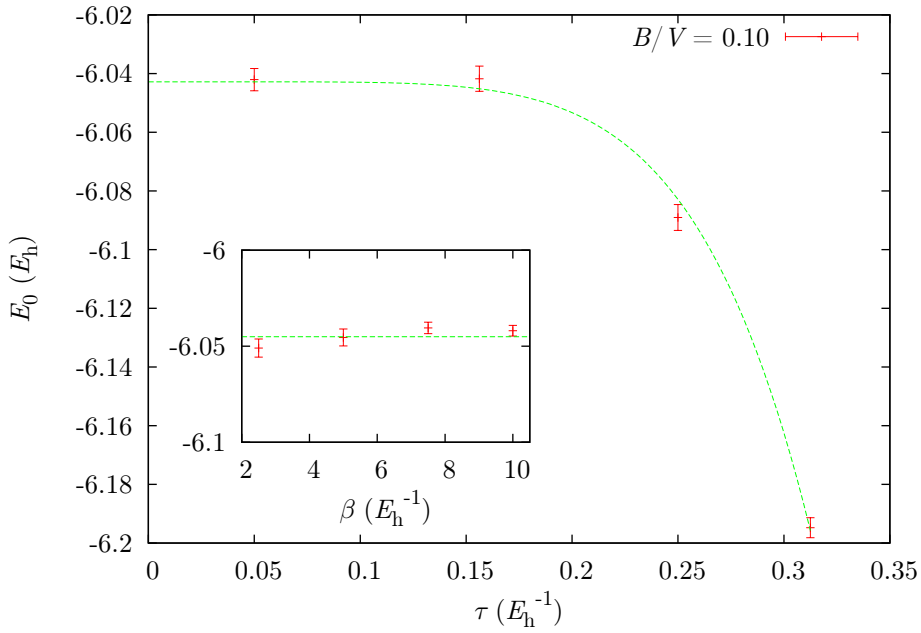

Figure 1: A plot of the ground state energy as a function of the small time step τ for a single stationary dipole in a constant electric field, with $V = d\,\|E\| = 10.0\ E_\mathrm{h}$ and a propagation time of $\beta = 5.0\ E_\mathrm{h}^{-1}$. The line is fit to a function of the form $E_0 = a + b\tau^6$ meant to highlight the convergence behavior. The inset shows the convergence of the energy with respect to the propagation time β at a time step $\tau = 5/56\ E_\mathrm{h}^{-1}$ where the dashed line shows the exact result.

Finding the proper values of β and τ entails finding a balance between accuracy and precision. Calculations can always be made more accurate by making β longer and τ shorter but this increases the number of time slices. This increases the number of beads that must be moved between one independent path and another, something that can be somewhat mitigated through the use of multibead moves. Since the error bars for a given simulation scale as $1/\sqrt{N}$ where N is the number of independent paths sampled, it's clear that there's a trade off between a desired accuracy, or how close to the true ground state of the system it is possible to probe, and a desired precision, the size of the error bars, given finite computer resources. Figure 1 shows the convergence behavior of the system with β and τ. For the current system, with $B/V = 0.10$, the value $\tau = 5/56\ E_\mathrm{h}^{-1}$ was found to be acceptable and the value $\beta = 2.5\ E_\mathrm{h}^{-1}$ was deemed suitably long for the given guiding wavefunction, $\psi_T = const.$

Once a sufficiently long β and sufficiently short τ are found then various properties and distribution functions of the ground state can be sampled. It was already shown in Figure 1 that the agreement in the energy calculation between PIGSMC and the basis set expansion calculation is excellent. Figure 2 shows the probability of finding the single dipole making an angle θ with respect to the positive z-axis. In this case the probability is

$$P(\theta) = \int_0^{2\pi} d\phi\, |\psi_0(\theta,\phi)|^2 \tag{49}$$

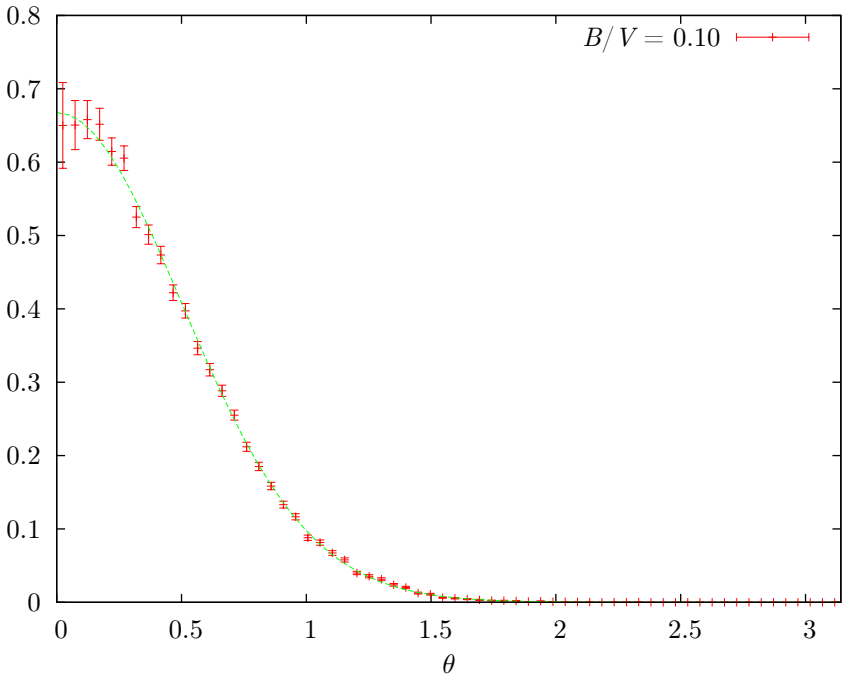

Figure 2: The probability, $P(\theta)$, of finding the single stationary rotor oriented with angle θ with respect to the electric field direction, along the positive z-axis. The dashed line is the exact result from the basis set expansion.

where $\psi_0(\theta, \phi)$ is the ground state wavefunction. This can be calculated exactly from the basis set expansion. If ν_0 is the normalized eigenvector which corresponds to the smallest eigenvalue of $\mathbf{H}$ then the probability is

$$P(\theta) = \left| \sum_{l=0}^{l_{max}} \nu_{0,l} \sqrt{\frac{2l+1}{4\pi}} \mathrm{P}_l(\cos(\theta)) \right|^2 \tag{50}$$

where $\mathrm{P}_l(\cos(\theta))$ are the Legendre polynomials. This function with $l_{max} = 128$ is plotted in Figure 2 as a dashed line, showing very good agreement with the PIGSMC result.

3.2 Two dipoles fixed in space with the dipole-dipole interaction

With the good agreement between the exact result and the PIGSMC result for a single stationary dipole in a constant electric field it is desirable to pursue a more complicated problem. After the problem of a singled fixed dipole in an external electric field, the problem of two identical dipoles with fixed positions interacting through the dipole-dipole interaction in the absence of an external field was the next simplest test case considered. The Hamiltonian describing this system is

$$\hat{H} = \sum_{i=1}^{2} B\hat{L}_i^2 + \frac{d^2}{4\pi\epsilon_0 r^3}(\hat{\mathbf{\Omega}}_1 \cdot \hat{\mathbf{\Omega}}_2 - 3(\hat{\mathbf{\Omega}}_1 \cdot \hat{r})(\hat{\mathbf{\Omega}}_2 \cdot \hat{r})) \tag{51}$$

where ϵ_0 is the vacuum permittivity (and $4\pi\epsilon_0$ will be taken to be 1), r is the distance between the two point dipoles, and $\hat{r}$ is the unit vector which joins the two point dipoles under consideration. Just as in the case of a single dipole in a constant electric field there

is only a single parameter $B/(d^2/r^3)$. Again the potential energy has the effect of aligning the two dipoles along the inter-dipole axis while the kinetic energy tends to delocalize the orientations of the two dipoles. When B is very large or d^2/r^3 is very small (*e.g.* by making the dipole moment very small or moving the dipoles further apart) then the case of two independent rotors is recovered and when B is very small compared to d^2/r^3 then the dipoles become more or less perfectly aligned.

Like the problem of a single dipole, analytical solutions to the time independent Schrödinger equation for this two body system are not available. Unlike that problem, however, the same type of basis set expansion as employed in the solution of that problem is more computationally costly since there are more degrees of freedom in this problem. A basis set expansion of the form

$$|\psi\rangle = \sum_{l_1=0}^{\infty} \sum_{m_1=-l_1}^{l_1} \sum_{l_2=0}^{\infty} \sum_{m_2=-l_2}^{l_2} c_{l_1,m_1}^{l_2,m_2} |l_1, m_1; l_2, m_2\rangle \tag{52}$$

truncated at some $l_{1,max} = l_{2,max} = l_{max}$ will contain $(l_{max}+1)^4$ states which means to find all of the expansion coefficients $c_{l_1,m_1}^{l_2,m_2}$ it is necessary to diagonalize a matrix with $(l_{max}+1)^8$ entries. For just $l_{max} = 10$ this is a 14641×14641, albeit sparse, matrix.

For smaller values of $B/(d^2/r^3)$, perturbation theory can be employed to calculate energies to compare with PIGSMC calculations. The ground state energy of the system up to second order in perturbation theory is

$$E_0 = E_0^{(0)} + E_0^{(1)} + E_0^{(2)} + \ldots \tag{53}$$

$$E_0^{(0)} = \langle 0, 0; 0, 0 | \hat{H}_0 | 0, 0; 0, 0 \rangle = 0 \tag{54}$$

$$E_0^{(1)} = \langle 0, 0; 0, 0 | \hat{V} | 0, 0; 0, 0 \rangle = 0 \tag{55}$$

$$E_0^{(2)} = \sum_{l_1=1}^{\infty} \sum_{m_1=-l_1}^{l_1} \sum_{l_2=1}^{\infty} \sum_{m_2=-l_2}^{l_2} \frac{|\langle l_1, m_1; l_2, m_2 | \hat{V} | 0, 0; 0, 0 \rangle|^2}{E_0^{(0)} - E^{(0)}(l_1, m_1; l_2, m_2)} \tag{56}$$

where $\hat{H}_0$ is the kinetic energy term and $\hat{V}$ is the dipole-dipole interaction potential. At first glance this does not appear any better than the variational calculation proposed above. However the expression $\langle l_1', m_1'; l_2', m_2' | \hat{V} | l_1, m_1; l_2, m_2 \rangle$ is only non-zero when $|l_1' - l_1| = 1$ and $|l_2' - l_2| = 1$ and so in the sum in equation (56) only a single term survives. To second order in perturbation theory the ground state energy of two stationary dipoles interacting through the dipole-dipole interaction is

$$E_0 \approx -\frac{d^4}{6Br^6} \tag{57}$$

which resembles a short range van der Waals type interaction.

As with the single dipole case, suitable values of β and τ must be found. Unlike the single dipole case there are no excited state energies to serve as guides for an initial value of β. An initial estimate of an appropriate β is the energy splitting in a system of two uncoupled rigid rotors, since the interaction energy in the case considered is assumed to be small compared to this. The exploration of appropriate values of β and τ then proceeded in an analogous fashion to the single dipole case. This is shown in Figure 3; the settled upon values of β and τ were 3.0 E_{h}^{-1} and 0.25 E_{h}^{-1} respectively. As with the problem of the single dipole, a constant guiding wavefunction was employed.

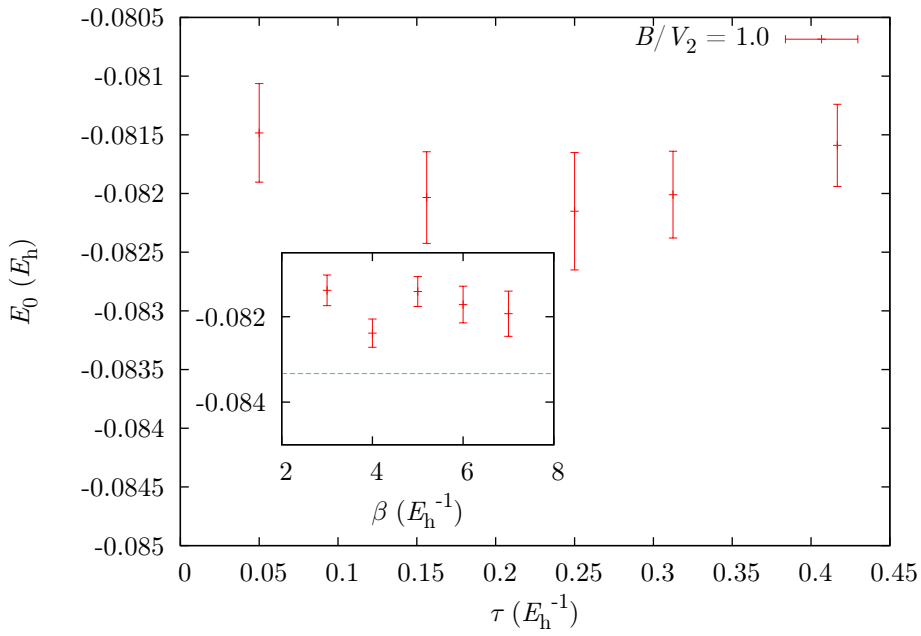

Figure 3: The energy per particle plotted as a function of the small time step τ for $B/V_2 = B/(d^2/r^3) = 1.0$. Clearly the energy has converged to within the error bars. The energy per particle plotted as a function of β for $\tau = 0.25\ E_h^{-1}$ is shown in the inset with a comparison to the perturbation theory result. The disparity between the PIGSMC and perturbation theory results is likely a consequence of the fact that the interaction potential $\hat{V}$ is comparable to the energy scale of the unperturbed states and in this parameter regime perturbation theory begins to break down.

There are three subspaces of minima in the potential energy for two stationary, rotating dipoles. The subspace of global minima of the potential energy occurs when two dipoles are oriented in the same direction along the axis joining the two dipoles and there are two such subspaces. A subspace of local minima occurs when both molecules are oriented perpendicular to the inter-dipole axis and are oriented anti-parallel to one another. For the rest of the discussion α will be taken as the angle between the two dipole orientations and the angle θ will be the angle an individual dipole makes with the inter-dipole axis. In a plot of the distribution of α and θ peaks are expected near the potential energy minima. Specifically there ought to be two peaks of approximately equal intensity for $\alpha = 0$ with $\theta = 0$ and π and a peak with less intensity centered around $\alpha = \pi$ with $\theta = \pi/2$.

This distribution is plotted in Figure 4 where these predictions are confirmed. For this parameter regime where the kinetic energy and potential energy are the same order of magnitude it is not surprising that the "peaks" are smeared out, the effect of the kinetic energy of the system.

3.3 Systems of many stationary dipoles

With the PIGSMC code proving itself on systems of one and two dipoles, the next logical step is to move onto systems of many dipoles fixed on a lattice. The Hamiltonian

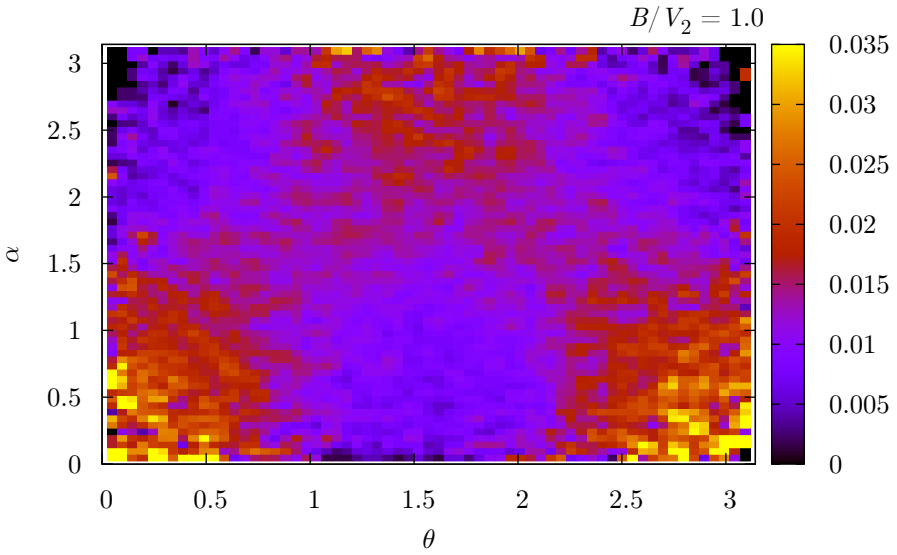

Figure 4: A plot of the distribution of α and θ. Notice the maxima near $\alpha = 0$ with $\theta = 0$ and π and $\alpha = \pi$ with $\theta = \pi/2$, as predicted.

describing a system of N dipoles on fixed lattice points is

$$\hat{H} = \sum_{i=1}^{N} B\hat{L}_i^2 + \sum_{i<j} \frac{d^2}{4\pi\epsilon_0 r_{ij}^3}(\hat{\mathbf{\Omega}}_i \cdot \hat{\mathbf{\Omega}}_j - 3(\hat{\mathbf{\Omega}}_i \cdot \hat{r}_{ij})(\hat{\mathbf{\Omega}}_j \cdot \hat{r}_{ij})) \tag{58}$$

which is just an extension of (51) where $r_{ij} = |r_i - r_j|$ is the distance between dipoles i and j. The behavior of this system is much less straight-forward than the other two cases considered. It is clear that if the interaction potential is weak compared to the kinetic energy of the system, $B/(d^2/r^3) \to \infty$, then the dipoles will be uncoupled and there should be no preferred orientation for any of the dipoles. In the opposite limit it really depends on the dimensionality of the lattice. In a one dimensional chain it seems natural that the preferred configuration should be the one in which all of the dipoles are aligned in the same direction along the axis of the chain. However, in two dimensions it is not at all clear which configuration will minimize the interaction potential and the problem of visualizing a minimum energy configuration is even more complicated in three dimensions. This is primarily because of the $1/r^3$ nature of the dipole-dipole interaction.

Applications of the PIGSMC code to these systems is an ongoing project but it will be very interesting to see what sorts of order appear in two dimensions. In addition it will be possible to study phase transitions which occur as the quantity $B/(d^2/r^3)$ is increased, from the unordered system of decoupled dipoles to some sort of ordered phase. This will like require the implementation of different types of non-local moves, such as cluster updates or the Worm algorithm [1], to deal with the divergence of correlation lengths near a hypothetical critical point. The data analysis techniques developed for these sorts of systems will hopefully lead to insight into how to study systems with additional degrees of freedom, such as translation in two and three dimensions.

4 Conclusion and outlook

A new PIGSMC code, the first of its kind, dealing with systems fully composed of rigid dipoles with rotational degrees of freedom was developed. It was shown that methods developed for translations can be applied to rotations in a relatively straightforward way. In order to apply the method, however, a few modifications were necessary. First, the free rotor propagator is not of a convenient form for on-the-fly evaluation unlike the free propagator and so it was necessary to tabulate this function at the beginning of the simulation and recall the values as needed. Still, a true sixth-order propagator for rotations was implemented.

The displacements of particles along the path is also slightly more complicated than the translational case since the orientations of linear molecular rotors are restricted to lie on the surface of the unit sphere. To alleviate these complications, unit quaternions were the representation of rotations used due to their ease of visualization and generation. It was then a simple matter to implement a multilevel Metropolis sampling algorithm for rotations.

The development of a PIGSMC code capable of simulating systems of rigid dipoles is an important step toward realistic calculations of the properties of molecular systems at ultracold temperatures. It opens to door to the observation of non-trivial many-body effects that arise from the coupling of translational and rotational degrees of freedom through the dipole-dipole interaction, which are not accessible through mean fields methods.

As experiment progresses the need for tools which can interpret experimental results as well as predict novel behavior will become more important. PIGSMC is poised to fill that role, being able to calculate exact properties of the ground state of many-body systems. It will also be possible to move beyond simple linear diatomic molecules as experiment progresses. It should be possible to extend this work to systems of polyatomic molecules in a straightforward fashion.

Acknowledgments

I'd like to acknowledge the Austrian Marshall Plan scholarship foundation for providing me the opportunity to travel to Linz in order to study with Robert Zillich. I'd also like to thank Johannes Mayrhofer, whose Monte Carlo code, developed under the supervision of Robert Zillich, was an invaluable reference for the development of the Monte Carlo code presented in the current work. Finally I'd like to thank Robert Zillich for his guidance in learning about quantum Monte Carlo.

References

[1] M. Boninsegni, N. Prokof'ev, and B. Svistunov, *Worm algorithm and diagrammatic Monte Carlo: A new approach to continuous-space path integral Monte Carlo simulations*, Physical Review E **74** (2006), no. 3, 1–16.

[2] Lincoln D. Carr, David DeMille, Roman V. Krems, and Jun Ye, *Cold and ultracold molecules: science, technology and applications*, New Journal of Physics **11** (2009), no. 5, 055049.

[3] D. Ceperley, *Path integrals in the theory of condensed helium*, Reviews of Modern Physics **67** (1995), no. 2, 279–355.

[4] Siu A. Chin, *Multi-product splitting and Runge-Kutta-Nystrom integrators*, arXiv:0809.0914v2 [math.NA] (2008), 1–14.

[5] D. DeMille, *Quantum Computation with Trapped Polar Molecules*, Physical Review Letters **88** (2002), no. 6, 067901.

[6] Eric Hudson, Christopher Ticknor, Brian Sawyer, Craig Taatjes, H. Lewandowski, J. Bochinski, J. Bohn, and Jun Ye, *Production of cold formaldehyde molecules for study and control of chemical reaction dynamics with hydroxyl radicals*, Physical Review A **73** (2006), no. 6, 6–11.

[7] Nicholas Metropolis, Arianna W. Rosenbluth, Marshall N. Rosenbluth, Augusta H. Teller, and Edward Teller, *Equation of State Calculations by Fast Computing Machines*, The Journal of Chemical Physics **21** (1953), no. 6, 1087.

[8] M. H. Müser and D. Marx, *Path integral simulations of rotors: theory and applications*, Journal of Physics: Condensed Matter (1999), no. 11, R117–R155.

[9] Shai Ronen, Daniele Bortolotti, and John Bohn, *Radial and Angular Rotons in Trapped Dipolar Gases*, Physical Review Letters **98** (2007), no. 3, 7–10.

[10] Robert E. Zillich, Johannes M. Mayrhofer, and Siu A. Chin, *Extrapolated High-Order Propagators for Path Integral Monte Carlo Simulations*, arXiv:0907.3495v1 [physics.comp-ph] (2009), 1–9.